Human-Robot Interaction Dynamics-Based Impedance Control Strategy for Enhancing Social Acceptance of Human-Following Robot

1st Jianwei Peng
Quanzhou Institute of Equipment Manufacturing
Fujian Institute of Research on the Structure of Matter, Chinese Academy of Sciences
Quanzhou, China
pengjianwei20@mails.ucas.ac.cn

2nd Zhelin Liao
Quanzhou Institute of Equipment Manufacturing
Fujian Institute of Research on the Structure of Matter, Chinese Academy of Sciences
Quanzhou, China
3211239023@fafu.edu.cn

3rd Zefan Su
Quanzhou Institute of Equipment Manufacturing
Fujian Institute of Research on the Structure of Matter, Chinese Academy of Sciences
Quanzhou, China
228527150@fzu.edu.cn

4th Hanchen Yao
Quanzhou Institute of Equipment Manufacturing
Fujian Institute of Research on the Structure of Matter, Chinese Academy of Sciences
Quanzhou, China
yaohanchen21@mails.ucas.ac.cn

5th Yadan Zeng*
The Robotics Research Centre of the School of Mechanical and Aerospace Engineering
Nanyang Technological University
Singapore
yadan001@e.ntu.edu.sg

6th Houde Dai*
Quanzhou Institute of Equipment Manufacturing
Fujian Institute of Research on the Structure of Matter, Chinese Academy of Sciences
Quanzhou, China
dhd@fjirsm.ac.cn

2023 China Automation Congress (CAC) | 979-8-3503-0375-9/23/$31.00 ©2023 IEEE | DOI: 10.1109/CAC59555.2023.10452070

***Abstract*—Human-following robots have gained widespread attention in diverse domains, such as manufacturing, healthcare, and personal companionship. However, it is essential to respect the social zones of the target person to avoid causing psychological discomfort when robots coexist and collaborate with humans. In this study, we propose a novel human-robot interaction dynamics-based impedance control strategy to accomplish the human-following task while ensuring that the robot refrains from encroaching upon the intimate zone of the target person. Initially, a human-robot interaction dynamics model is developed to capture the social repulsion between the robot and the target person. Subsequently, an impedance controller is designed to dynamically regulate the robot motion and the virtual interaction force with the target person. Furthermore, behavioral dynamics is integrated into the impedance controller for obstacle avoidance. Experimental results validate the effectiveness of the proposed method in this study, showcasing that the robot can successfully achieve human following and obstacle avoidance without encroaching on the intimate zone of the target person.**

***Index Terms*—human-following, impedance control, behavioral dynamics, human-robot interaction dynamics, obstacle avoidance**

I. Introduction

Human-following robots are gradually penetrating our daily lives, which can undertake various tasks ranging from transporting loads, offering companionship, and providing social support [1]. When a human-following robot collaborates with an individual in a shared workspace, it is essential for the robot to exhibit human-friendly behavior to ensure the security and comfort of the target person, which is crucial for the robot to gain acceptance from humans [2].

Generally, human-following control tasks encompass driving the robot to follow the target person, maintaining a safe distance, and avoiding obstacles [3]. Some previous research on human-following control has satisfactorily addressed these tasks. For instance, Yao et al. [4] developed a PID controller based on the estimated relative position and motion primitives of a human-following blimp. Similar control methods were also presented in [5]–[8]. Yuan et al. [9] proposed a control strategy based on artificial potential field, utilizing forces from potential fields to guide the robot in following the target person while avoiding obstacles. Additionally, Nguyen et al. [10] and Van et al. [11] intensively investigated fuzzy control-based human following and obstacle avoidance. However, these methods achieve the human-following task via single position or speed control, limiting their suitability to simple scenarios with limited performance. To this end, Ashe et al. [12] employed model predictive control to track the path of the target person and maintain a safe distance, but it lacks flexibility. Furthermore, Hirose et al. [13] proposed a predictive control policy involving deep neural network learning to accomplish the human-following task, but the stability and

Video demonstration: https://www.bilibili.com/video/BV1x14y1v7Cs

*Corresponding authors. This work was supported by the Natural Science Foundation of Fujian Province under Grant 2021J01388, the Fujian Science and Technology Project under Grant 2021Y0048, and the Quanzhou Science and Technology Project under Grant 2022C002L, 2022FX7, and 2022NS001.

security of this method remain uncertain. Notably, all of these approaches concentrate solely on the position control of the robot, neglecting the essential human factor, which is crucial for achieving a human-accepted human-robot interaction.

The study on proxemics by Hall et al. [14] reveals that individuals naturally maintain social zones during interactions to avoid causing psychological discomfort. Similarly, when a robot follows a person, it is perceived that the robot should also respect these social zones to enhance its social acceptance [15]. The interactive space between the robot and the person is divided into four zones, i.e., intimate zone (0-0.45m), personal zone (0.45-1.2m), social zone (1.2-3.6m), and public zone (>3.6m), based on their relative distance [16]. Moreover, to prevent causing psychological discomfort, the robot should avoid encroaching upon the intimate zone of the target person [2]. Therefore, Sekiguchi et al. [17] proposed an uncertainty-aware robot controller based on nonlinear model predictive control to maintain the robot position in the personal zone and avoiding obstruct human walking. However, this approach assumes a constant target person velocity, limiting its practicality. Furthermore, Herrera et al. [18] proposed that ensuring individual comfort involves not only respecting these social zones but also considering the dynamics during the interaction, i.e., treating these zones as flexible potential areas enables the robot to achieve a natural and smooth motion to ensure the comfort of individuals. To achieve this, they employed impedance control to establish human-robot interaction dynamics and enable compliant control for the human-following robot, thereby enhancing its social acceptance. However, this method does not incorporate heading angle control and neglects obstacle avoidance. Subsequently, Tian et al. [19] designed an obstacle avoidance component in the impedance control-based human-following controller, but it was limited to simulation.

Furthermore, obstacle avoidance is indispensable in the human-following task, as it ensures the robot can move safely and efficiently in real-world environments while guaranteeing the reliability of its human-following behavior. Regrettably, it has been overlooked in many previous studies (e.g., [2], [4], [5], [8], [18]). Moreover, research on human-robot interaction has indicated that the similarity between robots and humans in low-level behavioral patterns can effectively enhance the naturalness of the robot's behaviors, thus improving the interaction experience for individuals and boosting the social acceptance of the robot [20]. Nevertheless, common obstacle avoidance methods (e.g., [6], [10], [12]) tend to overlook this aspect. Hence, we favor the adoption of behavioral dynamics [21], which enables the robot to avoid obstacles by emulating human walking behavior.

Inspired by the aforementioned contributions, we propose a human-robot interaction dynamics-based impedance control strategy for human-following and obstacles avoidance, aiming to enable the robot to respect the social zones of the target person. At first, we construct a human-robot interaction dynamics model that captures the social repulsion between the robot and the target person. Subsequently, an impedance controller is designed to dynamically regulate the robot's motion and the virtual interaction force with the target person. Through this controller, the robot can effectively avoid encroaching upon the intimate zone of the target person, thereby ensuring their safety, comfort, and enhancing the social acceptance of the robot. Finally, we integrate an obstacle avoidance component based on behavioral dynamics into the impedance controller to further improve its practicality.

The main contributions are summarized as follows:

1) A human-robot interaction dynamics-based impedance control strategy can achieve human following while ensuring that the robot refrains from encroaching upon the target person's intimate zone.
2) A behavior dynamics-based obstacle avoidance component is integrated into the impedance controller, enhancing the naturalness of the robot motion and the practicality of the human-following controller.

II. Human-Robot Interaction Model

In this section, we characterize the kinematic and dynamic model of the human-following robot, which is a differential-driven mobile robot, as illustrated in Fig. 1. Furthermore, we introduce a human-robot interaction dynamics model based on virtual interaction force.

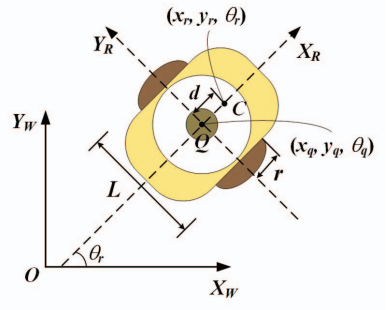

Fig. 1. Model schematic of the human-following robot.

A. Modeling Robot Motion

We denote the centroid of the robot $[x_r, y_r, \theta_r]^T$ as its pose, with $[x_q, y_q, \theta_q]^T$ representing the coordinate of the robot's wheel axle center. The differential-driven mobile robot satisfies the nonholonomic constrains, thus the kinematics of the robot can be described by [22]

$$\begin{bmatrix} \dot{x}_r \\ \dot{y}_r \\ \dot{\theta}_r \end{bmatrix} = \begin{bmatrix} cos\theta_r & dsin\theta_r \\ sin\theta_r & -dcos\theta_r \\ 0 & 1 \end{bmatrix} \begin{bmatrix} v \\ w \end{bmatrix}, \tag{1}$$

where d is the distance between the robot's wheel axle center and its centroid. v and w are the linear and angular velocities of the robot, respectively.

Consider referencing the dynamics of the differential-driven mobile robot as defined in [23]:

$$\begin{bmatrix} \dot{x}_r \\ \dot{y}_r \\ \dot{\theta}_r \\ \dot{v}_r \\ \dot{w}_r \end{bmatrix} = \begin{bmatrix} vcos\theta_r - dwsin\theta_r \\ vsin\theta_r + dwcos\theta_r \\ w \\ -v\Psi_2/\Psi_1 \\ -w\Psi_4/\Psi_3 \end{bmatrix} + \begin{bmatrix} 0 & 0 \\ 0 & 0 \\ 0 & 0 \\ 1/\Psi_1 & 0 \\ 0 & 1/\Psi_3 \end{bmatrix} \begin{bmatrix} v \\ w \end{bmatrix}, \tag{2}$$

where $(\Psi_1, \Psi_2, \Psi_3, \Psi_4)$ are the parameters of the robot model,

$$\Psi_1 = \frac{mr^2R_a + 2rK_a + 2I_eR_a}{2rK_a}, \Psi_2 = \frac{rK_a + K_aK_b + B_eR_a}{rK_a},$$
$$\Psi_3 = \frac{2r^2IR_a + 2rLK_a + LI_eR_a}{2rLK_a},$$
$$\Psi_4 = \frac{2rK_a + LK_aK_b + B_eR_a}{2rK_a},$$

m is the mass of the robot, r is the radius of the wheels, L is the distance between drive wheels, I is the rotational inertia of the robot, K_a is the product of the motor torque constant and the gear transmission ratio, K_b is the product of the motor voltage constant and the gear transmission ratio of the motor, R_a is the resistance constant, I_e is the rotational inertia of the wheel, and B_e is the damping coefficient of the drive wheel.

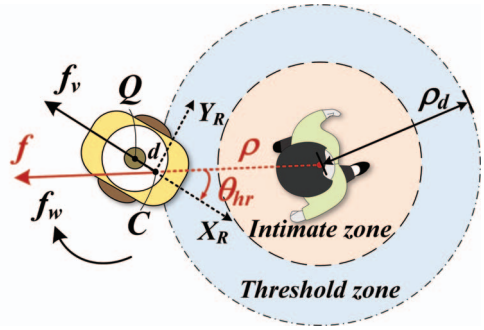

Fig. 2. Human-robot interaction dynamics.

B. Human-Robot Interaction Dynamics Model

Human-robot interaction dynamics utilize non-physical forces to characterize the dynamic interaction relationship between the robot and the person. It assumes the existence of a hypothetical potential field within the individual's intimate zone. If the robot encroaches upon this zone while following the target person, it encounters a repulsive force that pushes it away from the intimate zone. The repulsion force on the robot within the target person's intimate zone can be expressed as [18]

$$f = \begin{cases} \gamma \frac{e^{-\frac{\rho^n}{\rho_d}} - e^{-\rho_d^{n-1}}}{1 - e^{-\rho_d^{n-1}}}, & \rho \le \rho_d \\ 0, & \rho > \rho_d \end{cases}, \tag{3}$$

where γ is denoted as gain, n is the pending index, ρ is the distance between the robot and the target person, and ρ_d is the desired distance and the range of interaction forces.

To ensure human comfort, we design a threshold zone slightly larger than the intimate zone, as depicted in Fig. 2. Additionally, the desired human-following distance (ρ_d) of the robot corresponds to the radius of the threshold zone. When the distance (ρ) between the robot and the target person is less than this desired distance (ρ_d), a virtual repulsive interaction force will be applied, compelling the robot to move away from that zone. Furthermore, the virtual interaction force can be composed as

$$f_s = [-fcos\theta_{hr}, -fdsin\theta_{hr}]^T, \tag{4}$$

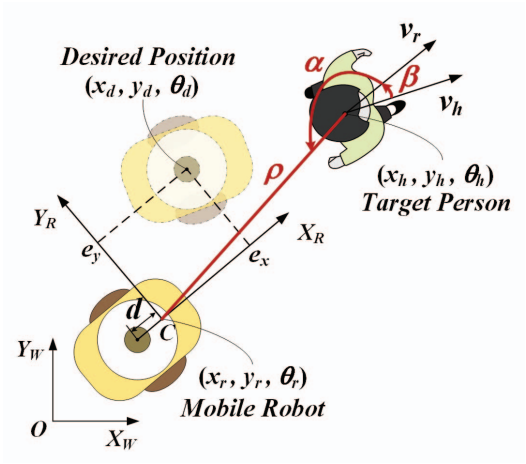

Fig. 3. Diagram of the human-following system. ρ is the distance between the robot and the target person, α is formed by the red connection line and the human orientation, and β is the relative orientation between the robot and the target person. e_x and e_y are the error between the desired position and the current position of the robot in the body-fix frame.

where $f_s = [f_v, f_w]^T$ are the components of in the forward and rotational of the robot, respectively. θ_{hr} is the azimuth angle of the human in the robot body-fixed frame.

III. Human-following Control Strategy

A. Human-following Control Objective Establishment

The state of the target person is denoted as $[x_h, y_h, \theta_h, v_h, w_h]^T$, where (x_h, θ_h) and θ_h are the position and orientation, respectively. v_h and w_h represent the forward and turning velocities of the target person, respectively. As depicted in Fig. 3, the robot is supposed to follow the target person with a desired separation ρ_d, a desired relative bearing α_d, and a desired relative orientation β_d. And we define the state of the human-following system as $S := [\rho, \alpha, \beta]^T$. Thus, the human-following control objective can be mathematized as

$$\lim_{t\to\infty} |S - S_d| = 0. \tag{5}$$

Moreover, the desired position of the human-following robot $[x_d, y_d, \theta_d]^T$ is determined by the desired system state and the posture of the target person, as

$$\begin{cases} x_d = x_h + \rho_d cos(\alpha_d + \theta_h) \\ y_d = y_h + \rho_d sin(\alpha_d + \theta_h) \\ \theta_d = \theta_h + \beta_d \end{cases}, \tag{6}$$

where $\alpha_d = \pi$, $\beta_d = 0$, and ρ_d is the preset distance for the robot to follow the target person and also the radius of the threshold zone.

B. Impedance Control-Based Human-following Controller

Impedance control is employed to characterize the dynamic relationship between the human-robot interaction force and the position of the robot with respect to the target person. The impedance control law is given by

$$I\ddot{X}_e + B\dot{X}_e + KX_e = -F_e, \tag{7}$$

where $F_e = F_d - F_i$ is the virtual interaction force deviation, F_d is the desired interaction force, and F_i is the actual interaction force between the robot and the target person, which is given by (3). $X_e = X_r - X_d$, X_r and X_d are the desired position and actual position of the robot, respectively. $I = diag(i,i)$, $B = diag(b,b)$, and $K = diag(k,k)$ are inertia, damping, and elastic matrix, respectively. Thus, we can obtain

$$\ddot{X}_r = I^{-1}(-F_e - B\dot{X}_e - KX_e) + \ddot{X}_d, \tag{8}$$

where $\ddot{X}_d$ can be calculated by (6) as

$$\ddot{X}_d = \begin{bmatrix} \ddot{x}_h - \rho_d\dot{\theta}_h^2 cos(\alpha_d + \theta_h) - \rho_d\ddot{\theta}_h sin(\alpha_d + \theta_h) \\ \ddot{y}_h - \rho_d\dot{\theta}_h^2 sin(\alpha_d + \theta_h) + \rho_d\ddot{\theta}_h cos(\alpha_d + \theta_h) \end{bmatrix}. \tag{9}$$

Furthermore, the impedance controller output vector X_r is defined by the robot's position, as $X_r = [x_r, y_r]^T$. Then according to the dynamics model of the robot (2), we can derive the first and second order time derivatives of the output

$$\begin{cases} \dot{X}_r = [\dot{x}_r, \dot{y}_r]^T = Au_r \\ \ddot{X}_r = [\ddot{x}_r, \ddot{y}_r]^T = E + A(G + Hu_d) \end{cases}, \tag{10}$$

where $u_r = [v, w]^T$ is the velocity vector of the robot, $u_d = [v_d, w_d]^T$ is the velocity references,

$$A = \begin{bmatrix} cos\theta_r & -dsin\theta_r \\ sin\theta_r & dcos\theta_r \end{bmatrix}, E = \begin{bmatrix} -vsin\theta_r - dwcos\theta_r \\ vcos\theta_r - dwsin\theta_r \end{bmatrix},$$
$$G = \begin{bmatrix} -v\Psi_2/\Psi_1 \\ -w\Psi_4/\Psi_3 \end{bmatrix}, H = \begin{bmatrix} 1/\Psi_1 & 0 \\ 0 & 1/\Psi_3 \end{bmatrix}.$$

Subsequently, applying feedback linearization [18] to the system based on (9) yields

$$u_d = H^{-1}\left[A^{-1}(u - E) - G\right]. \tag{11}$$

Substituting (8) into (11) yields the impedance control law for human-following

$$u_d = H^{-1}\left[A^{-1}(I^{-1}(F_i - B\dot{X}_e - KX_e) + \ddot{X}_d - E) - G\right]. \tag{12}$$

Moreover, the coordination of motion between the robot and the target person is critical in human-following behavior, requiring the robot to track the direction of the target person, i.e., $\lim_{t\to\infty}|\beta_d| = 0$.. However, incorporating the control of the robot's heading angle in the impedance controller becomes complex due to the coupling between the robot's heading angle and position.

Therefore, we design an angular velocity compensator, as

$$\mu = \begin{cases} 0, & X_e > \delta \\ K_w\beta, & X_e \le \delta \end{cases}, \tag{13}$$

where K_w is the angular velocity compensator gain, $\beta = \theta_d - \theta_r$ is the robot heading angle deviation, and $\delta = \left[e_x^\delta, e_y^\delta\right]^T$ is a threshold for the robot position error. The robot prioritizes tracking the position of the target to maintain the formation. When the robot's position error X_e is less than the threshold δ, the angular velocity compensator kicks in to enable the robot to track the direction of the target person more accurately and stably.

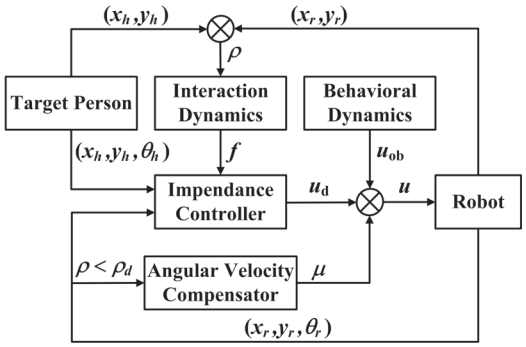

Fig. 4. Schematic diagram of the control strategy for human-following and obstacle avoidance.

Consequently, by synthesizing (12) and (13), we can obtain the impedance control-based compliant human-following controller

$$u_{hfr} = u_d + [0 \quad 1]^T \mu. \tag{14}$$

C. Behavioral Dynamics-Based Obstacle Avoidance

By analyzing human walking behavior, researchers have discovered that individuals primarily adjust the direction of their forward movement to bypass obstacles, with the influence of the relative direction and distance of the obstacles to the individual [19], [21]. Therefore, Fajen et al. [21] proposed a behavioral dynamics-based obstacle avoidance method that enables robots to emulate human obstacle avoidance behavior. And the formula for behavioral dynamics is as

$$\ddot{\theta}_{ob} = \begin{cases} -k_0\zeta e^{-c_1|\zeta|}e^{-c_2 d_{ob}}, & d_{ob} \le d_s \\ 0, & d_{ob} > d_s \end{cases}, \tag{15}$$

where $\ddot{\theta}_{ob}$ is the output of the obstacle avoidance component, ζ is the orientation angle of the obstacle relative to the robot, d_{ob} is the distance from the robot to the obstacle, d_s is the safe distance, $k_0 > 0$, $c_1 > 0$, and $c_2 > 0$ are gains. Notably, $e^{-c_1|\zeta|}$ is the component produced by the orientation angle of the obstacle with respect to the robot, and $e^{-c_2 d_{ob}}$ is the component produced by the relative distance between the obstacle and the robot.

Assume that there are n_{ob} obstacles, and w_{ob}^i is the angular velocity component produced by the $i-th$ obstacle, which can be obtained by integrating (15). Thus, the output of the obstacle avoidance component can be written as

$$u_{ob} = \begin{bmatrix} 0 & \sum_{i=1}^{n_{ob}} w_{ob}^i \end{bmatrix}^T. \tag{16}$$

Integrating the obstacle avoidance control input (15) into the impedance controller (13) yields the human-following and obstacle avoidance control law

$$u_{ob} = u_{hfr} + u_{ob}, \tag{17}$$

and the schematic diagram of the control strategy is shown in Fig. 4.

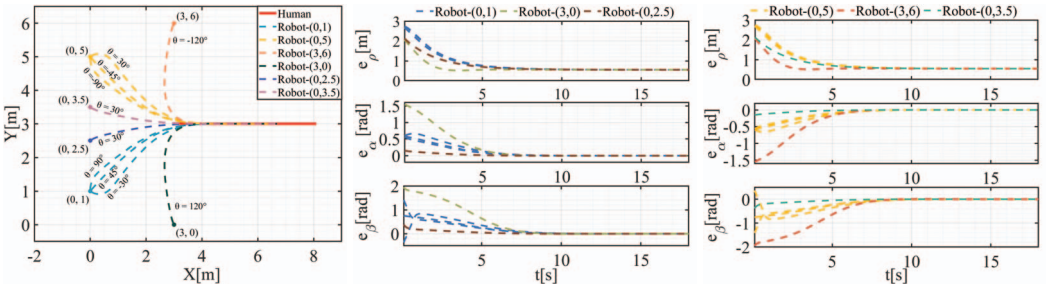

(a) Trajectories (b) State error (c) State error

Fig. 6. Simulation for the human-following. The robot follows the target person from behind with various initial states.

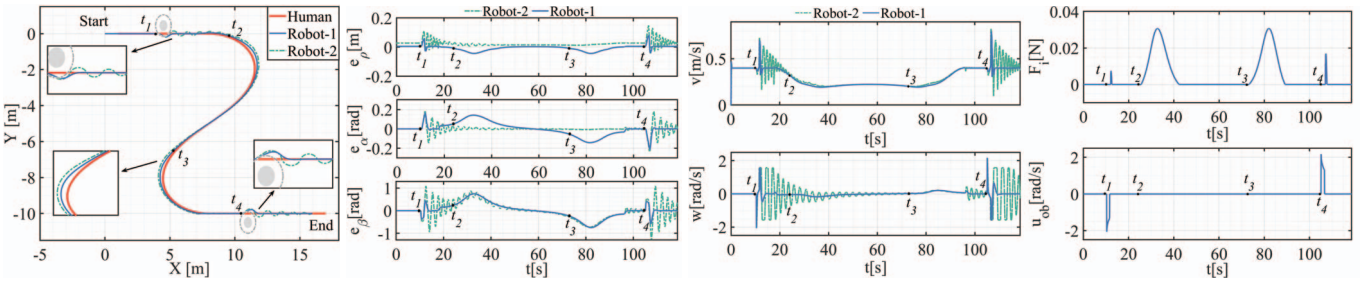

(a) Trajectories (b) State error (c) Velocity (d) F_i and u_{ob}

Fig. 7. Simulation for the human-following and obstacle avoidance. Robot-1 is the experimental results of the robot following the target person with angular velocity compensator, and Robot-2 is the experimental results without angular velocity compensator.

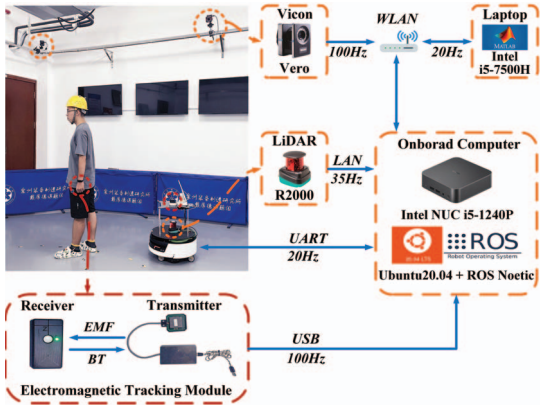

Fig. 5. Experiment setup. EMF: electromagnetic field. BT: Bluetooth. The EMTM transmitter is mounted on the robot. The receiver is worn by the target person. Vicon is utilized to capture the trajectory of the robot and the target person, and LiDAR for detecting obstacles.

IV. Experiments And Results

A. Experimental Setup

The simulation experiments of the human-following task were performed in MATLAB 2021b to validate the effectiveness of the proposed method. The experimental parameters are listed in Table I. Furthermore, to rapidly demonstrate the feasibility of our control strategy in real-world scenarios, we established a master-slave network by connecting MATLAB to Robot Operating System (ROS, noetic), as illustrated in Fig. 5. Within this network, the control algorithm runs in MATLAB, and control commands are transmitted from ROS to the robot's actuator. Simultaneously, ROS feeds sensor data to MATLAB. Specifically, we employ an electromagnetic tracking module (EMTM, https://www.amfitech.dk/) to directly acquire the position and orientation of the target person. The closed-loop system operates at a frequency of 20Hz.

TABLE I
EXPERIMENTAL PARAMETERS

Parameter	Value	Parameter	Value	Parameter	Value
m/kg	40	Ψ_1	0.03	k	0.2
r/m	0.216	Ψ_2	0.10	K_w	1.50
L/m	0.525	Ψ_3	0.10	δ	[0.1; 0.1]
d/m	0.04	Ψ_4	0.10	k_0	60
ρ_d/m	1.00	i	0.008	c_1	0.42
d_s/m	0.60	b	0.05	c_2	0.10

B. Simulation Results

To validate the effectiveness of our proposed method, we conducted two sets of simulation experiments. In the first set, we set the trajectory of the target person as a straight line (red line) starting from (3, 3) and moving along the positive direction of the X-axis, as shown in Fig. 6(a). The robot started following the target person from behind in various positions and initial angles. The state error curves of the human-following system in Fig. 6(b) and Fig. 6(c) indicate that the robot can steadily track the target person and converge the state error to zero in a reasonable time.

In the second set of experiments, we generated an S-shaped trajectory for the target person with variations in direction and velocity and set up obstacles. The blue trajectory (Robot-1) in Fig. 7(a) represents the robot's trajectory under the control of our method, and the blue curves in Fig. 7(b) depict the system state error. The robot effectively maintained the system states at the desired values, with significant deviations occurring only during obstacle avoidance and the target person changed direction, which were quickly re-converged. Additionally, in Fig. 7(c), the robot responded compliantly during the interaction, smoothing out its motion changes and demonstrating the compliance of impedance control. Notably, during avoiding obstacles (e.g., t_1 and t_4) and when the target person changed direction (e.g., t_2 and t_3), the robot sometimes encroached

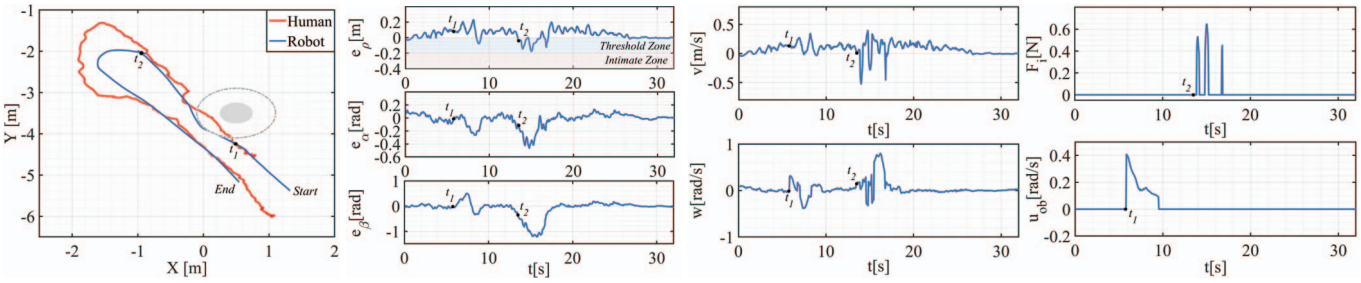

(a) Trajectories (b) State error (c) Velocity (d) F_i and u_{ob}

Fig. 9. Experiment for human-following and obstacle avoidance. At t_1, the robot avoids the obstacle in its path. At t_2, the robot unintentionally encroaches into the target person's threshold zone when the target person makes a 180-degree turn. The gray circle and the gray dotted line in (a) represent the obstacle and the safe range of the obstacle, respectively. The blue zone and pink zone in (b) are the threshold zone and intimate zone of the target person, respectively.

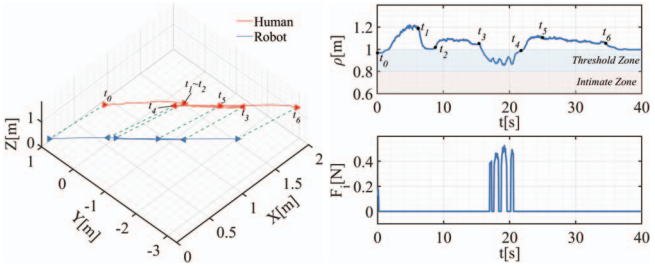

(a) Trajectories (b) State error

Fig. 8. Human-following experiment involving the target person walking along a straight line with motion mutations. The green dashed lines in (a) are the line connecting the position of the robot and the target person at a given time. The triangles in (a) represent the position and direction of the robot and the target person at a given moment in time. The blue zone and pink zone in (b) are the threshold zone and intimate zone of the target person, respectively.

upon the threshold zone of the target person (i.e., $\rho \leq \rho_d$). However, as shown in Fig. 7(d), the robot experienced an interaction force that pushed it away from the threshold zone, effectively preventing encroachment into the intimate zone of the target person.

Furthermore, to demonstrate the effect of the angular velocity compensator, we conducted an experiment without angular velocity compensator, as depicted in Robot-2 in Fig. 7. In this case, the robot failed to promptly regulate the heading angle after avoiding the obstacle, resulting in oscillations that could potentially lead to the failure of the human-following task or even safety issues in real-world scenarios. Moreover, the robot exhibited slower responses when the target person changed direction.

C. Real-World Experiments Results

The experiment setup is illustrated in Fig. 5. In the experiment depicted in Fig. 8, the target person walked along a straight line, making abrupt stops at t_1, moving forward at t_2 and t_4, briefly stepping back at t_3 to approach the robot, and ultimately coming to a halt at t_6. Despite these variations in the target person's motion, the robot exhibited smooth and responsive behaviors, effectively tracking the target person's motion. Moreover, as shown in Fig. 8(b), when the robot entered the threshold zone of the target person, it was prevented by a repulsive force F_i from further encroaching on the target person's intimate zone (e.g., t_0 and $t_3 - t_4$). This ensured that the robot maintained a safe and respectful distance from the target person, improving the comfort of the target person and enhancing social acceptance of the human-following robot.

Furthermore, to further validate the performance of the proposed control strategy in generalized scenarios, we also conducted the experiment as depicted in Fig. 9. During this experiment, the robot avoided the obstacle while following the target person, effectively accomplishing the desired task. Additionally, when the target person turned, the repulsive force prevented the robot from encroaching further into the target person's intimate zone, thereby safeguarding the comfort of the target person and ensuring the robot's human-friendly behavior. These experimental results demonstrate the versatility and efficacy of the proposed method in real-world scenarios.

V. Conclusions

In this study, we propose a human-following control strategy based on impedance control and human-robot interaction dynamics, which effectively respects the social zone of the target person during the human-following process, leading to improved comfort for the target person and enhanced social acceptance of the robot. Firstly, a human-robot interaction dynamics model is employed to capture the social repulsion between the robot and the target person. The human-following controller is designed based on the human-robot interaction dynamics using impedance control, which can dynamically regulate the robot motion and virtual interaction force with the target person. Secondly, integrating an obstacle avoidance component based on behavioral dynamics improves the naturalness and practicality of our method. Specifically, using an EMTM to directly acquire the target person's position and orientation enhances the precision and efficiency of our system. Experimental results showcase the effectiveness of the proposed control strategy, demonstrating that the robot can smoothly follow the target person, navigate around obstacles, and refrain from encroaching upon the intimate zone of the target person.

However, we acknowledge that the current parameters of our controllers were obtained through empirical tuning, potentially limiting adaptability in different scenarios. To address this limitation, we intend to explore adaptive control strategies in future research, enabling the system to dynamically adjust its parameters based on real-time feedback and environmental conditions.

REFERENCES

[1] S. Li, K. Milligan, P. Blythe, Y. Zhang, S. Edwards, N. Palmarini, L. Corner, Y. Ji, F. Zhang, and A. Namdeo, "Exploring the role of human-following robots in supporting the mobility and wellbeing of older people," *Scientific Reports*, vol. 13, no. 1, p. 6512, 2023.

[2] S. Sekiguchi, A. Yorozu, K. Kuno, M. Okada, Y. Watanabe, and M. Takahashi, "Human-friendly control system design for two-wheeled service robot with optimal control approach," *Robotics and Autonomous Systems*, vol. 131, p. 103562, 2020.

[3] M. J. Islam, J. Hong, and J. Sattar, "Person-following by autonomous robots: A categorical overview," *The International Journal of Robotics Research*, vol. 38, no. 14, pp. 1581–1618, 2019.

[4] N. Yao, E. Anaya, Q. Tao, S. Cho, H. Zheng, and F. Zhang, "Monocular vision-based human following on miniature robotic blimp," in *2017 IEEE International Conference on Robotics and Automation (ICRA)*. IEEE, 2017, pp. 3244–3249.

[5] S. Su, S. Cheng, H. Dai, M. Lin, H. Yu, and J. Zhang, "An efficient human-following method by fusing kernelized correlation filter and depth information for mobile robot," in *2019 IEEE International Conference on Robotics and Biomimetics (ROBIO)*. IEEE, 2019, pp. 2099–2104.

[6] J. Chen and W.-j. Kim, "A human-following mobile robot providing natural and universal interfaces for control with wireless electronic devices," *IEEE/ASME Transactions on Mechatronics*, vol. 24, no. 5, pp. 2377–2385, 2019.

[7] H. Yao, H. Dai, E. Zhao, P. Liu, and R. Zhao, "Laser-based side-by-side following for human-following robots," in *2021 IEEE/RSJ International Conference on Intelligent Robots and Systems (IROS)*. IEEE, 2021, pp. 2651–2656.

[8] G. Xue, H. Yao, Y. Zhang, J. Huang, L. Zhu, and H. Dai, "Uwb-based adaptable side-by-side following for human-following robots," in *2022 IEEE International Conference on Robotics and Biomimetics (ROBIO)*. IEEE, 2022, pp. 333–338.

[9] J. Yuan, S. Zhang, Q. Sun, G. Liu, and J. Cai, "Laser-based intersection-aware human following with a mobile robot in indoor environments," *IEEE Transactions on Systems, Man, and Cybernetics: Systems*, vol. 51, no. 1, pp. 354–369, 2018.

[10] T. V. Nguyen, M. H. Do, and J. Jo, "Robust-adaptive-behavior strategy for human-following robots in unknown environments based on fuzzy inference mechanism," *Industrial Robot: the international journal of robotics research and application*, vol. 49, no. 6, pp. 1089–1100, 2022.

[11] N. Van Toan, M. Do Hoang, P. B. Khoi, and S.-Y. Yi, "The human-following strategy for mobile robots in mixed environments," *Robotics and Autonomous Systems*, vol. 160, p. 104317, 2023.

[12] A. K. Ashe and K. M. Krishna, "Maneuvering intersections & occlusions using mpc-based prioritized tracking for differential drive person following robot," in *2021 IEEE 17th International Conference on Automation Science and Engineering (CASE)*. IEEE, 2021, pp. 1352–1357.

[13] N. Hirose, R. Tajima, and K. Sukigara, "Mpc policy learning using dnn for human following control without collision," *Advanced Robotics*, vol. 32, no. 3, pp. 148–159, 2018.

[14] E. T. Hall, "A system for the notation of proxemic behavior," *American anthropologist*, vol. 65, no. 5, pp. 1003–1026, 1963.

[15] J. Rios-Martinez, A. Spalanzani, and C. Laugier, "From proxemics theory to socially-aware navigation: A survey," *International Journal of Social Robotics*, vol. 7, pp. 137–153, 2015.

[16] X.-T. Truong, V. N. Yoong, and T.-D. Ngo, "Dynamic social zone for human safety in human-robot shared workspaces," in *2014 11th International Conference on Ubiquitous Robots and Ambient Intelligence (URAI)*. IEEE, 2014, pp. 391–396.

[17] S. Sekiguchi, A. Yorozu, K. Kuno, M. Okada, Y. Watanabe, and M. Takahashi, "Uncertainty-aware non-linear model predictive control for human-following companion robot," in *2021 IEEE International Conference on Robotics and Automation (ICRA)*. IEEE, 2021, pp. 8316–8322.

[18] D. Herrera, F. Roberti, M. Toibero, and R. Carelli, "Human interaction dynamics for its use in mobile robotics: Impedance control for leader-follower formation," *IEEE/CAA Journal of Automatica Sinica*, vol. 4, no. 4, pp. 696–703, 2017.

[19] H. Tian and X. Ma, "Behavioral dynamics-based impedance control for collision avoidance of human-following robots," in *2022 IEEE International Conference on Real-time Computing and Robotics (RCAR)*. IEEE, 2022, pp. 349–354.

[20] T. Kruse, A. K. Pandey, R. Alami, and A. Kirsch, "Human-aware robot navigation: A survey," *Robotics and Autonomous Systems*, vol. 61, no. 12, pp. 1726–1743, 2013.

[21] B. R. Fajen and W. H. Warren, "Behavioral dynamics of steering, obstable avoidance, and route selection." *Journal of Experimental Psychology: Human Perception and Performance*, vol. 29, no. 2, p. 343, 2003.

[22] R. Fierro and F. L. Lewis, "Control of a nonholomic mobile robot: Backstepping kinematics into dynamics," *Journal of robotic systems*, vol. 14, no. 3, pp. 149–163, 1997.

[23] C. De La Cruz and R. Carelli, "Dynamic modeling and centralized formation control of mobile robots," in *IECON 2006-32nd annual conference on IEEE industrial electronics*. IEEE, 2006, pp. 3880–3885.